ENERGY JITTER MINIMIZATION AT LCLS*

Lanfa Wang#, Timothy Maxwell, Franz-Josef Decker, Andrew Benwell, Axel Brachmann, Anatoly Krasnykh, Zhirong Huang, James Turner, William Colocho, Tang Tao
SLAC, Stanford, CA 94309, USA

Abstract

The energy jitter of the electron beam affects FELs in self-seeded modes if the jitter is large compared to the FEL parameter, effectively reducing the average brightness when shots are seeded off-energy. We work in multiple ways to reduce jitter, including hardware improvement and optimizing linac set-up. Experiments demonstrated better than 20% and 40% relative energy jitter reduction for 13.6 and 4 GeV linac operation, respectively. This paper discusses the global optimization of linac set-up using Multi-Objective Genetic Algorithm (MOGA). The solutions always suggest that we can largely reduce the energy jitter from a weak compression at BC1 and a stronger compression at BC2. Meanwhile low beam energy at BC2 also reduces the energy jitter, which is confirmed by the experiment.

INTRODUCTION

The impact of energy jitter on self-seeded FELs is understood by considering the flux transmitted through an X-ray monochromator. Assuming SASE with Gaussian bandwidth σ_{SASE} incident on a monochromator, the ratio F of off-energy transmitted X-ray flux to on-energy flux due to *rms* electron relative energy jitter σ_e is given by

$$F(\sigma_e) = \frac{\sigma_{SASE}}{\sqrt{\sigma_{SASE}^2 + 4\sigma_e^2}}. \quad (1)$$

For self-seeding, this implies the average available seed power degrades unless $\sigma_e << \sigma_{SASE} / 2$. Should sufficient undulator length be available to reach post-saturation, slightly weaker seed intensities can in principle be stabilized to near-nominal in post-mono amplification. In this way, self-seeding can be slightly more robust against energy jitter vs. direct SASE filtering alone.

Figure 1 illustrates this energy dependence during the 2014 development of soft X-ray self-seeding (SXRSS) at the LCLS [1] at 540 eV. The fraction of X-ray power within twice the self-seeded bandwidth plotted as a function of δe shows the 0.12% rms energy jitter yields a 50% reduction of the average narrow-band X-ray intensity (0.1 vs. 0.2 mJ). Therefore, improving linac energy stability has the potential double the average spectral brightness achievable by SXRSS.

Over the years the beam stability and jitter have been investigated [2-7] to study and identify jitter sources and improve stability of the LCLS. Over recent years, a group of experts worked together to improve the energy jitter, including improving klystron station stability and other hardware, automated data logging, developing online linear models, etc. Experiments demonstrated better than 25% and 40% relative energy jitter reduction for 13.6 and 4 GeV linac operation, respectively, over the past year.

Here we present our global optimization of the linac to reduce the machine energy jitter. The simulation model and the optimized solutions for hard x-ray and soft x-ray beams are discussed in the following sections. Hardware upgrades will be briefly discussed towards the end.

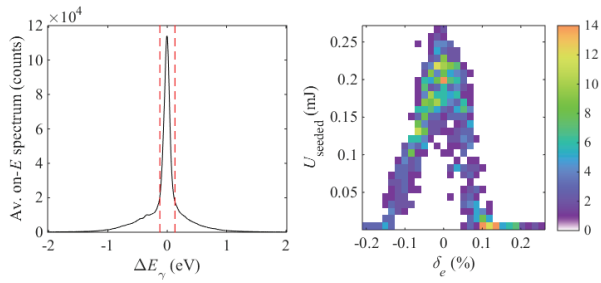

Figure 1: Average on-energy SXRSS spectra and range of fractional integration range (left). 2D histogram of partial pulse intensities U_{seeded} as a function of δ_e (right).

JITTER SOURCE AND SIMULATION MODEL

The primary source of the jitter is from the linac rf. The variation of pulse-to-pulse energy and timing jitter accumulates along the linac, each station adding in quadrature, and therefore has a large impact on beam jitter. Timing jitter at an rf station induces energy jitter as

$$\delta E(\varphi_0) = -e\omega_{rf}\hat{V}sin(\varphi_0)\delta t. \quad (2)$$

Additionally, amplitude fluctuations of rf klystrons along the linac generate an additional term to beam energy jitter as

$$\delta E(\varphi_0) = -e\hat{V}sin(\varphi_0)\delta\varphi + ecos(\varphi_0)\delta\hat{V}. \quad (3)$$

The first and secondary term on the left of the equation comes from the phase jitter and voltage jitter, respectively. For off-crest acceleration prior to bunch compression, the dominant contribution of the beam energy jitter is the beam timing/phase jitter at the rf stations as shown in Eq. 2. This timing jitter works similar as the rf phase jitter. Its effective rf phase jitter is

$$\delta\varphi_{rf,eff} = \omega_{rf}\delta t \quad (4)$$

*Work supported by Department of Energy Contract No. DE-AC02-76SF00515
#wanglf@SLAC.stanford.edu

ISBN 978-3-95450-134-2

However, the timing jitter seen at each rf station is not purely localized, being accumulated from upstream acceleration. For given rf phase and voltage jitter, we can optimize the linac configuration to reduce the energy jitter by minimizing the timing jitter effect in Eq. 2.

The magnet in bunch compressors (BCs) has very good stability and its jitter has negligible impact on the beam energy jitter. However BC acts as a dispersive element, converting energy jitter to correlated timing jitter. The effective *E-t* correlation provided by a BC is

$$\left(\frac{\delta E/E}{\delta t}\right)_{BC} = c/R_{56}, \quad (5)$$

where c is the speed of light in vacuum and R_{56} is the momentum compaction factor of the BC. Since R_{56} at BC is negative, it contributes to a negative chirp.

Finally the collective effects such as wakefields and coherent synchrotron radiation (CSR) also add to the energy jitter through the jitters of bunch charge and current profile. These effects are not simply formulized.

As discussed above, the rf and BC elements can be treated as linear system for small variation. We can approximate the machine as a simple linear system to estimate jitter in the absence of nonlinear effects and collective effects. To fully and accurately optimize the machine, Multi-Objective Genetic Algorithm (MOGA) is applied to optimize the machine parameters in order to minimize the jitters (timing jitter, energy jitter and current jitter), energy spread and collective effects and provide zero energy chirp and certain peak current at the end of linac. For instance the overall jitters is defined as

$$jitter^2 = \sum_i \left[\frac{(\delta I/I)_i^2}{(\delta I/I)_0^2} w_I + \frac{(\delta E/E)_i^2}{(\delta E/E)_0^2} w_E + \frac{(\delta t/t)_i^2}{(\delta t/t)_0^2} w_T\right], \quad (6)$$

where $w_{I,E,T}$ are the weight factors for current, energy and timing jitter. The sum on the left is over all runs (seeds). The particles are tracked using LiTrack code in this paper, which includes the wakefields. But CSR and space charge are not modelled.

HARD X-RAY

Table 1 lists two optimized solutions for hard x-ray beam with a small energy jitter and 3 kA peak current. The configuration close to old operational configuration is also listed for comparison (The machine configuration change rapidly to improve the performance). The two optimized solutions are for 5.0 GeV and 6.3 GeV beam energy at BC2, respectively. There are about 100% improvements in energy jitter for both two fully optimized solutions.

The final beam before the undulator for solution 1 is shown in Fig. 2. The phase space is also optimized to get zero energy chirp. The current profile is similar as the nominal one. It has flat top at the core part of beam with horns at both head and tail of the bunch. Fig. 3 shows the detail of the jitters for the case with zero L3 phase. The energy jitters are widely distributed with large contributions from the phase of L1S, L2 and L1X. The total rms energy jitter is 0.01%.

The timing and energy jitter in general is correlated. This correlation comes primarily from the uncorrelated jitter growth from rf phase and voltage jitters being stretched by compression R_{56}. Fig. 4(left) shows the energy and timing jitter for solution 1 when L3 phase is set to zero. Apparently there is a correlation between the energy jitter and rf phase jitter. The relation between the beam energy jitter and beam timing jitter observed at each rf station is $\delta\varphi = \omega_{rf}\delta t$. If we define the correlation between the energy and timing jitter as $h = (\delta E/E)/\delta t$, then the *E-t* correlation provided by rf linac is

$$\left(\frac{\delta E/E}{\delta t}\right)_{rf} = -e\omega_{rf}\hat{V}sin(\varphi_0)/E \quad (7)$$

here E is the beam energy at that element. Therefore we can apply an appropriate rf phase at L3 to conceal the residual correlation and provide the same energy gain. This correlation can be minimized to zero by setting a non-zero *L3* phase so that the final energy jitter is a minimal:

$$\varphi_{L3} = atan\left[\frac{E}{\omega_{rf}\hat{V}_{L30}} h_0\right]. \quad (8)$$

Where $\hat{V}_{L30}$ is the *L3* voltage with zero rf phase and h_0 is the E-t correlation when L3 phase is set to zero. In the derivative of Eq. 8 we assume the whole L3 has the same rf phase. In operation, the rf phase along the L3 varies. But the idea is the same: the E-t chirper provided the L3 totally conceal the original chirper h_0 from upstream. For different operation modes, this *E-t* correlation and the beam energy gain at L3 varies. Therefore the optimal L3 phase also changes.

Co-author Decker first proposed the above idea at the LCLS to reduce the energy jitter which we refer to as "Decker phasing." The underlying physics of Decker phasing is to remove correlated energy jitter via L3 chirp. Fig.4(right) shows the E-t jitter with an optimal L3 phase of -13.8^o, where the final E-t correlation becomes zero. The final energy jitter is about 21% smaller compared to the case with zero L3 phase. The detail dependence of energy jitter on the L3 phase is shown in Fig. 5.

The major changes of the optimized solution includes L2 phase and R_{56}. A smaller L2 phase and $|R_{56}|$ at BC1 is prefered. With the same jitter sources, the energy jitter with the nominal configuration is about 0.022%. Therefore the optimized solution reduces the energy jitter to only 36% of that with nominal configuration. The improvement is significant.

Figure 6-7 shows the impact of L3 phase for the nominal configuration. There is a minimum energy jitter at L3 phase of –20 degree. Fig. 8 shows the observed dependence of energy jitter on the L3 phase. There is large improvement (25%) at the optimal L3 phase of

ISBN 978-3-95450-134-2

Table 1: Example of LCLS Operational and Optimized Solutions for Hard X-Ray

Variables	Solution1	Solution2	~old operational
BC2 energy(GeV)	5.0	6.3	5.0
I_{pk} (kA)	3.0	3.0	3.0
Charge(pC)	150	150	150
V_{0A}(MV)	57.5	57.5	57.7
V_{0B}(MV)	71.5	71.5	71.5
ϕ_{0A} (degree)	0	0	–5
ϕ_{0B} (degree)	–5	–5	–5
ϕ_{L1} (degree)	–29.85	–27.8	–26.1
V_{L1S}(MV)	125	122	118
ϕ_{Lx} (degree)	–159.4	–157	–160
V_{Lx}(MV)	25	25	22
ϕ_{L2} (degree)	–19.5	–19.5	–38.7
V_{L2}(GV)	5.0758	6.455	6.15
ϕ_{L3} (degree)	–13.8	–10.8	–20
V_{L3}(GV)	8.9	10.7	8.778
R_{56}@BC1(mm)	–35.4	–36	–45.5
R_{56}@BC2(mm)	–47.3	–47.1	–20.6
(Δt) (fs)	26	26	22
(ΔE/E) (%)	0.0078	0.0082	0.022

range from –14 to –20 degree. The simulation agrees reasonably well with the experiment.

There is a possibility to increase the LCLS final beam energy by increasing the rf acceleration at L2 and therefore the beam energy at BC2. We assume that the beam energy at BC2 is 6.3 GeV so we can have the maximum final beam energy up to 17.0 GeV [8]. The 2nd solution at Table 1 shows the main parameters of such solution. This solution (except rf voltage at L2 and L3) is close to solution 1 and the jitters are also similar to that solution. The energy jitter is about 0.010% and 0.0082% with zero and –10.8 degree L3 phase, respectively. Fig. 9 shows the solution in detail.

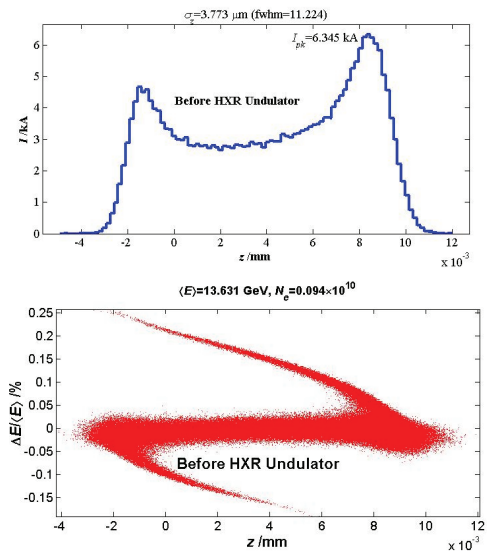

Figure 2: The final beam before the undulator listed for solution 1 in Table1. The beam energy at BC1 and BC2 is 220MeV and 5GeV, respectively. The final beam energy is 13.6GeV. Bunch lead is to the left.

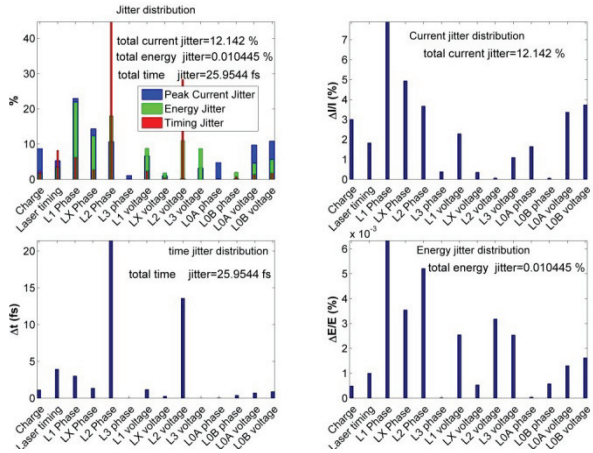

Figure 3: The distributions of jitters in energy, timing and current for the solution 1. But the L3 phase is zero in this study.

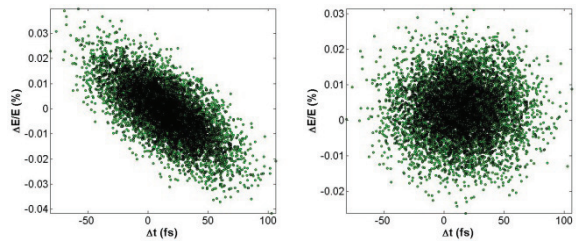

Figure 4: The energy and timing jitter at the end of linac for solution 1 with different L3 phases: 0 (left, energy jitter 0.01%) and –13.8° (right, energy jitter 0.0078%).

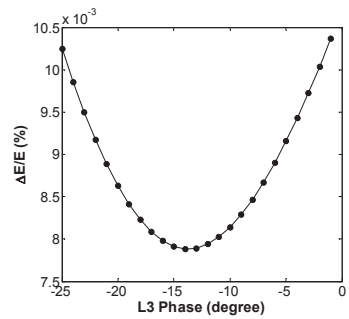

Figure 5: Simulated effect of L3 phase on the energy jitter for the optimized solution 1. The optimized L3 phase is –13.8 degree.

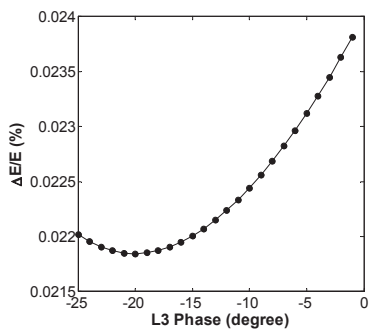

Figure 6: Simulated effect of L3 phase on the energy jitter for the old operational configuration. The optimized L3 phase is –20 degree.

ISBN 978-3-95450-134-2

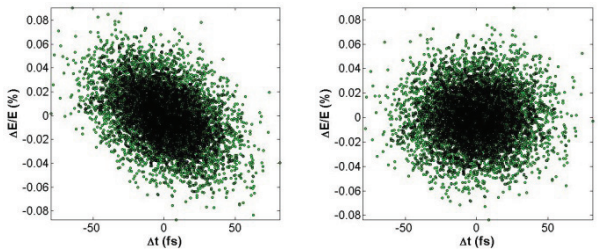

Figure. 7: Simulated effect of L3 phase on the energy jitter for the old operational configuration listed in Table 1. The L3 phase is zero (left) and –20 degree (right), respectively.

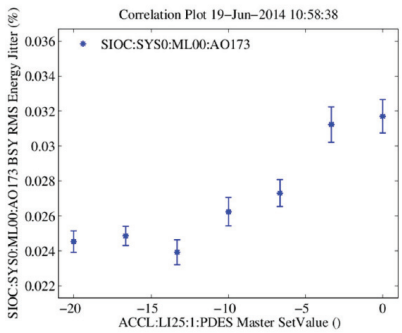

Figure 8: Observed energy jitter for different L3 phase for hard x-ray beam on June 19 of 2014.

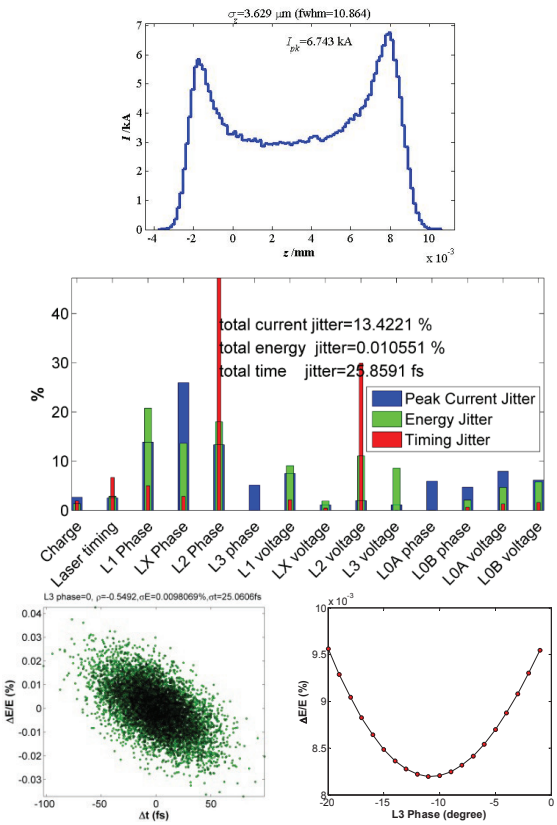

Figure 9: Current profile (top), jitters (middle) and impact of L3 phase on energy jitter (bottom) for solution 2 with beam energy of 6.3 GeV at BC2. The final beam energy is 17.0 GeV.

SOFT X-RAY

In LCLS the beam energy at the 2nd bunch compressor (BC2) is historically fixed at 5.0 GeV for both hard X-ray and soft X-ray beams. For example for a soft x-ray beam energy of 3.0 GeV, the beam is decelerated by linac 3 (L3) from 5.0 GeV to 3.0 GeV. In this way, for practical reasons, we fix the machine set-up before BC2 and use only L3 to adjust the final beam energy.

Simulation has shown that lower beam energy at BC2 can reduce the energy jitter for low energy running. We simply reduce the beam energy at BC2 from 5.0 GeV to 3.5 GeV while the finally beam energy at the end of linac is kept the same 3.5 GeV. In the first case the L3 decelerates the beam from 5.0 GeV to 3.5 GeV (left column of Fig. 10), while it does nothing in the 2nd case (right column of Fig. 10). In both cases the R_{56} at BC2 is set to –24.7 mm and the L2 phase is adjusted to get 1.5 kA current at the core of the beam shown in Fig. 10. The energy jitter reduces from 0.076% to 0.044% when the beam energy at BC2 is reduced from 5.0 GeV to 3.5 GeV.

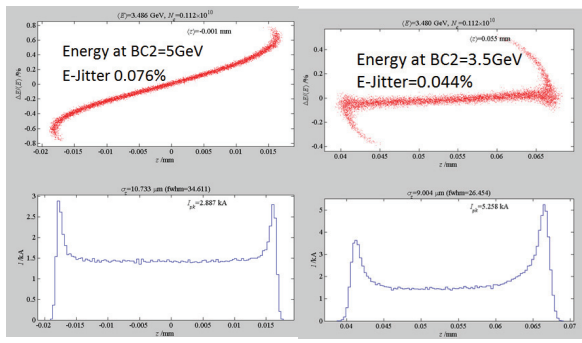

Figure 10: Simulated beam and energy jitter with different beam energy at BC2: 5.0 GeV(left) and 3.5 GeV (right). The final beam energy is 3.5GeV in both cases.

The strong dependence of the energy jitter on the beam energy at BC2 is confirmed by the experiment as shown in Fig. 11. The beam energy at BC2 is gradually reduced from 5.0 GeV to 3.5 GeV. The final beam energy is kept at 4.0 GeV by adjusted the rf at L3. Meanwhile the rf phase at L2 is adjusted (by the feedback) to keep a peak current of 1.5 kA. The *rms* energy jitter is reduced from 0.11% to 0.08%, about 27% improvement (top of the figure). Then the R_{56} at BC2 is adjusted from –24.7 mm to –27.2 mm, there is no apparent jitter impact. In the previous steps, the rf phase of L3 is kept at 0 phase (on crest). Finally the rf phase of L3 is changed to –15°. There is no clear impact on the jitter, which can be explained by the insufficient E-t correlation provide by L3 (Eq. 7). We will discuss more on that aspect shortly.

Both simulation and experiments show improvement of energy jitter with low beam energy at BC2. From quasi-linear theory including individual klystron station jitter contributions adding in quadrature in an *E-t* correlated fashion, it is clear a large jitter reduction stems from the dramatically reduced number of L2 and L3 rf stations (22 vs. 32) needed to achieve the final beam energy of 4 GeV

ISBN 978-3-95450-134-2

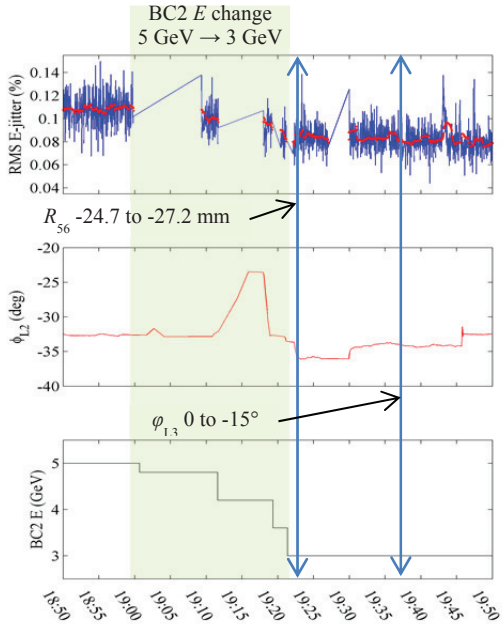

Figure 11: Observed energy jitter in LCLS when we scan the beam energy at BC2. The R56 at BC2 (1st line) and the rf phase of L3 (2nd line) are also adjusted to verify impact on the jitter. The figure shows the final energy jitter (top), the rf phase of L2 (middle) and the beam energy at BC2 (bottom), respectively.

by not over-accelerating in L2 leading to a 30-40% jitter reduction now used in low-*E* operation by fixing BC2 energy at 3 GeV if L3 energy is < 6 GeV. This approach yields jitter numbers consistent in scale with experimental results, but models only jitter evolution for a given configuration not including individual bunch longitudinal dynamics, collective effects such as wakefields, or optimization of final chirp. In the MOGA approach, we optimize the LCLS linac for different beam energies at BC2 with each linac treated as one rf station, and including wake effects. Table 2 shows two optimized solutions (1st and 2nd column) and the one close to the old operational mode (3rd column).

There are additional improvements in the energy jitter for the two further optimized solutions compared to the old operational configuration. These large improvements are the integrated effects of the optimized machine and are even better than the one with reduced BC2 energy alone (0.044%, Fig. 10). The beam energy at BC2 is 3.0 GeV and 5.0 GeV for the solution 1 and 2 respectively with similar energy jitters for the two sets of optimized solutions. We find the energy jitter can be even further reduced by full optimization under the condition of avoiding over-acceleration of the beam.

The beam and energy jitter of the three configurations are shown in Fig. 12-14. There are the same beam current of 1.5 kA at the core part of beam for all cases. There clear difference in the phase space, especially the energy chirp. Current "horns" for the old operational mode are small, indicating our machine is well tuned for that purpose.

The configurations in Table 2 do not apply Decker phasing. There are clear correlations between the energy and timing jitter in all cases. In principle the energy jitter can be further reduced using Decker phasing similar to the hard x-ray case. The required L3 rf phase is much larger (far away from crest) due to a low energy gain (or loss) at L3 for soft x-ray beam. As shown in Eq. 7-8, a large phase is required for Decker phasing if the rf voltage is low. It is also confirmed by the simulations shown in Fig. 12-14. A much large L3 phase (more than 60 degree) is required. This may explain the observation at LCLS where weak Decker phasing doesn't help much for soft x-ray beam when rf phase of L3 is varied only with 20 degree from the crest. Apparently this phase is not sufficient.

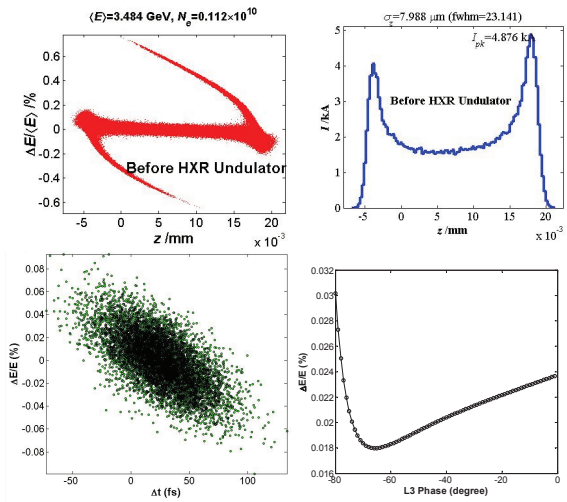

Figure 12: Beam and energy jitter of solution 1 as shown in Table 2: longitudinal phase space (top left); current profile (top right); energy and timing jitters when the L3 phase is zero (bottom left); impact of L3 phase on the energy jitter (bottom right).

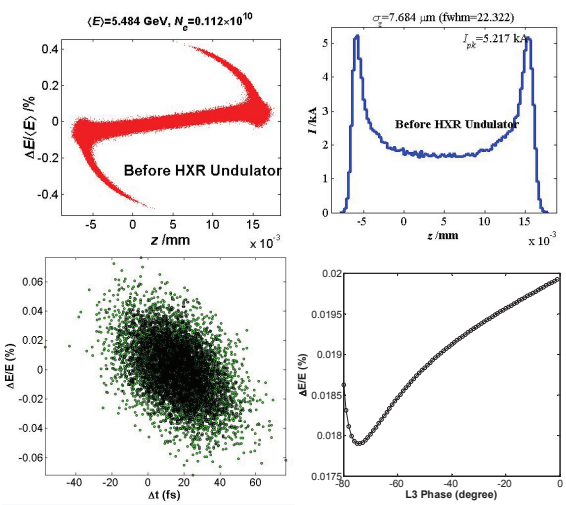

Figure 13: Beam and energy jitter of solution 2 as shown in Table 2: longitudinal phase space (top left); current profile (top right); energy and timing jitters when the L3 phase is zero (bottom left); impact of L3 phase on the energy jitter (bottom right).

ISBN 978-3-95450-134-2

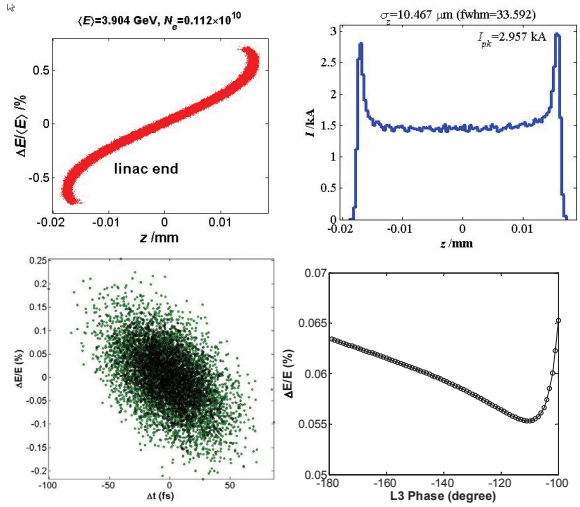

Figure 14: Beam and energy jitter with operational confiuration as shown in Table 2: longitudinal phase space (top left); current profile (top right); energy and timing jitters when the L3 phase is −180° (bottom left); impact of L3 phase on the energy jitter (bottom right).

Table 2: Examples of Two Fully Optimized Solutions for Soft X-Ray and Operational Configuration

Variables	Solution1	Solution2	*~operational*
E at BC2(GeV)	*3.0*	*5.0*	5.0
Final E (GeV)	*3.5*	*5.5*	3.9
I_{pk} (kA)	1.5	1.5	*1.5*
Charge(pC)	180	180	*180*
V_{0A}(MV)	57.5	57.5	*57.5*
V_{0B}(MV)	71.9	71.9	*71.9*
ϕ_{0A} (degree)	0	0	*–0*
ϕ_{0B} (degree)	–5	–5	*–5*
ϕ_{L1} (degree)	–26.7	–27.35	*–27.2*
V_{L1S}(MV)	119	120	*115*
ϕ_{Lx} (degree)	–159	–159.8	*–160*
V_{Lx}(MV)	23	23	*18.2*
ϕ_{L2} (degree)	–21.47	–19.5	*–34.2*
V_{L2}(GV)	2.987	5.058	*5.79*
ϕ_{L3} (degree)	–0	–0	*–180*
V_{L3}(GV)	0.5	0.5	*1.086*
R_{56}@BC1(mm)	–35.1	–36.7	*–45.5*
R_{56}@BC2(mm)	–47.6	–47.1	*–24.7*
(Δt) (fs)	27	15	*23*
(ΔE/E) (%)	0.024	0.020	*0.0635*

HARDWARE IMPROVEMENTS

Beyond optimization of the linac configuration, underlying hardware instability has also been carefully scrutinized and improved over recent years [4-7, 9-11]. Some of these have included regular maintenance of critical injector stations from the rf gun through the first bunch compressor. These "seed" significant downstream energy jitter growth as the first compressor converts incoming energy jitter into a phase jitter, increasing susceptibility to energy jitter growth due to phase instability in linac 2.

One item under development is improved high-power RF loads. With gradual SLAC klystron improvements over the years, the peak power klystron output has been raised to > 20 MW. The existing 2 MW SLAC RF loads no longer provide stable termination, as shown in Fig. 15 (top). Unstable reflected power is found to interfere in the later portion of the RF pulse. This issue is exacerbated in SLED mode operation shown with randomly fluctuating reflected power interfering with beam-time RF.

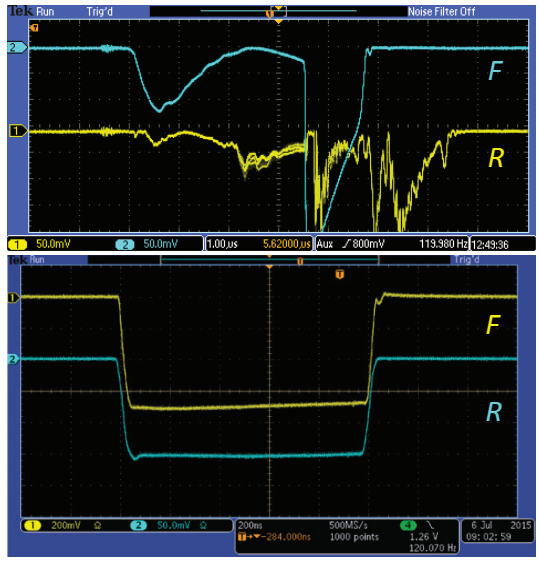

Figure 15: Scope traces of Forward and Reflected RF power for a SLEDed SLAC rf station with 2 MW SLAC RF old (top) and unSLEDed station with new, 20 MW SLAC RF load (bottom).

In answer to this, SLAC has developed a 20 MW-class, all-metal RF load. High-power RF conditioning of the first two loads has been successfully completed, with results from the first complete load shown in Fig. 15 (bottom) [10,11]. This shows stable RF termination at over 18 MW peak forward power for 1 μs pulses at 120 Hz stably terminated at 3 kW average. Upgrade of critical, SLEDed injector stations is currently being planned with long term roll out to remaining LCLS sectors under evaluation.

Additionally we are investigating the upgrade from hydrogen thyratrons to new, deuterium thyratrons with a higher beam voltage rating. The hydrogen thyratrons currently in use are run at > 90% of their maximum rating of 47 kV for the majority of stations. These results in frequent thyratron ranging and replacement resulting in degraded station performance and increased cost. In contrast, the thyratron driving the LCLS gun is operated at lower voltage (78% derated) and has run with excellent stability without thyratron replacement for over 20 years.

The deuterium thyratron replacement is plug compatible and rated for 80 kV @ 1 kHz while also auto-ranging. One has been in operation on a non-critical LCLS station for over 6 months showing a 48% improvement to pulse forming network stability, 30% reduction of beam voltage jitter, and with output phase and amplitude jitter reduced to present measurement limits while requiring no thyratron maintenance since

ISBN 978-3-95450-134-2

installation. This also is under consideration for rollout to critical injector stations with potential deployment to the remainder of the LCLS linac over future years.

SUMMARY AND DISCUSSION

The global computer optimizations have been done to minimize the energy jitter in LCLS. The benefit of low beam energy at BC2 is confirmed by experiment. The measured energy jitter for soft x-ray is improved about 27% by reducing the beam energy at BC2 from 5.0 GeV to 3.0 GeV.

We also confirm that "Decker phasing" can be used at L3 to conceal the residual E-t correlation for hard x-ray case. The optimal phase of –20 degree is close to the experiment. The experiment shows a larger reduction of 25% in energy jitter. Decker phasing is explained by a simple formula for a given residual correlation between energy and timing jitters. Studies show that a much large L3 phase is required for soft x-ray beam "Decker phasing". We will test that in the machine.

The global optimizations for the whole linac show significant energy jitter reduction (from 2.2×10^{-4} to 8×10^{-5} for hard x-ray beam and from 6.4×10^{-4} to 2.4×10^{-4} for soft x-ray beam). We will explore these solutions to further improve the jitter. Besides Decker phasing and lower beam energy at BC2 for soft X-ray operation, other ideas to reduce the energy jitter proposed include:

- *Reduce the compression (R56) at the first BC (BC1) and increase the compression (R56) at the 2nd BC (BC2).*
- *Reduce the rf phase of L2*

The maximum |R56| at BC2 is limited by the power supply of the magnets. We can operationally set the R56 of BC2 close to its maximum and optimize other parameters.

The simulations agree reasonable well with the observations with guidance for improving stability. Recent improvements in hardware should also reduce jitter while reducing maintenance. Since the sources of jitters vary time to time, it is more accurate and also straight forward to do online optimization to incorporate known, present sources of instability while maximizing the requested FEL performance simultaneously. A better simulation model, such as including CSR, will be updated. The online and off-line start-to-end optimization is our plan for next step along with ongoing hardware improvements.

ACKNOWLEDGEMENTS

This work is supported by Department of Energy Contract No. DE-AC02-76SF00515.

REFERENCES

[1] D. Ratner, et al., Phys. Rev. Lett. 114, 054801 (2015).
[2] P. Emma, J. Wu, "Trajectory Stability Modelling and Tolerances in the LCLS", EPAC06 Edinburgh, p.151.
[3] R. Akre et al., "Beam Stability Studies in the LCLS Linac", FEL08, Korea, Aug 2008.
[4] F.-J. Decker, et al., "Identifying Jitter Sources in the LCLS Linac", Linac08, Victoria, BC, Canada, p. 506.
[5] F.-J. Decker, et al., "Improving Beam Stability in the LCLS Linac", PAC09, Vancouver, BC, Canada, 2009, p. 2349.
[6] F.-J. Decker, et al., "Identifying Longitudinal Jitter Sources in the LCLS Linac", IPAC'10, Kyoto, Japan, 2010, p. 2296.
[7] F.-J. Decker, et. al., Increased Stability Requirements for Seeded Beams at LCLS, WEPSO10, in the proceedings of the 35th International Free-Electron Laser (FEL 2013).
[8] F.-J. Decker, et. al., Photon Energies beyond the Selenium K-Edge at LCLS, WEP022, these proceedings.
[9] F.-J. Decker, A. Krasnykh, B. Morris, and M.Nguyen, "A stability of LCLS Linac Modulators", SLAC-PUB-15083.
[10] A. Krasnykh, et. al., S-Band loads for SLAC Linac, MOPB087, in Proceedings of LINAC2012, Tel-Aviv, Israel.
[11] A. Krasnykh, et. al., online at http://slac.stanford.edu/pubs/slacwps/wp06/slac-wp-099.pdf

ISBN 978-3-95450-134-2